AGU PUBLICATIONS

Geophysical Research Letters

RESEARCH LETTER
10.1002/2017GL075189

Key Points:
- Example of ionospheric irregularities in the Martian ionosphere below 200 km altitude is presented
- Statistical analysis of similar events shows peak occurrences at dawn and dusk
- Cause of irregularities is unclear, particularly as irregularities appear to be electromagnetic in nature

Correspondence to:
C. M. Fowler,
christopher.fowler@lasp.colorado.edu

Citation:
Fowler, C. M., Andersson, L., Shaver, S. R., Thayer, J. P., Huba, J. P., Lillis, R. J. . . . Jakosky, B. M. (2017). MAVEN observations of ionospheric irregularities at Mars. *Geophysical Research Letters*, *44*, 10,845–10,854. https://doi.org/10.1002/2017GL075189

Received 7 AUG 2017
Accepted 10 OCT 2017
Accepted article online 24 OCT 2017
Published online 4 NOV 2017

MAVEN Observations of Ionospheric Irregularities at Mars

C. M. Fowler[1], L. Andersson[1], S. R. Shaver[1], J. P. Thayer[2], J. D. Huba[3], R. Lillis[4], M. E. Usanova[1], J. Espley[5], R. E. Ergun[1], J. Mcfadden[4], P. R. Mahaffy[6], J. E. P. Connerney[5], M. Benna[5,7], M. Elrod[8], D. L. Mitchell[4], C. Mazelle[9], and B. M. Jakosky[1]

[1]Laboratory for Atmospheric and Space Physics, University of Colorado Boulder, Boulder, CO, USA, [2]Department of Aerospace Engineering Sciences, University of Colorado Boulder, Boulder, CO, USA, [3]Plasma Physics Division, Naval Research Laboratory, Washington, DC, USA, [4]Space Sciences Laboratory, University of California, Berkeley, CA, USA, [5]Planetary Magnetospheres Lab, NASA Goddard Space Flight Center, Greenbelt, MD, USA, [6]Planetary Environments Laboratory, NASA Goddard Space Flight Center, Greenbelt, MD, USA, [7]CRESST, University of Maryland, Baltimore, MD, USA, [8]Planetary Environments Laboratory, NASA Goddard Space Flight Center, Greenbelt, MD, USA, [9]IRAP, University of Toulouse, CNRS, UPS, CNES, Toulouse, France

Abstract Ionospheric irregularities associated with horizontal magnetic fields below 200 km altitude are observed at Mars. Plasma density modulations of up to 200% are observed during such events and appear correlated with fluctuations in the magnetic field. The observed fluctuations are likely Doppler shifted and represent spatial structures at length scales of 15–20 km or less. Conditions in the Martian ionosphere below 200 km are synonymous with the terrestrial *E* region, where ionospheric irregularities have been extensively studied. Interestingly, the irregularities at Mars appear to be electromagnetic in nature, in contrast to the electrostatic nature of irregularities at Earth. It is currently unclear what the primary drivers of these irregularities at Mars are, and further study is needed to explain these important phenomenon within the Martian ionosphere.

1. Introduction

In situ observations of the Martian ionosphere began in the late 1970s with the two Viking Landers. Both landing sites were at solar zenith angles (SZA) close to about 44°; Viking 1 landed at about 4 p.m. local time and Viking 2 at about 10 a.m. (e.g., Nier & McElroy, 1977). In situ measurements made by the retarding potential analyzers carried by both landers were the first of their kind to be made at Mars and provided critical insight into the structure, composition, and energetics the dayside Martian ionosphere and neutral atmosphere. The ionospheric peak was observed just below 130 km altitude with a density of $\sim 10^5$ cm^{-3}. O_2^+ made up about 90% of the ionospheric density there (Hanson et al., 1977).

The Mars Global Surveyor (MGS) mission was the first spacecraft to orbit Mars that repeatedly sampled the Martian ionosphere. It arrived at Mars in late 1997 and stayed on orbit through most of 2006 until contact was lost with the spacecraft. The instrumentation suite carried by MGS was focused on remotely sensing the surface of Mars, and as such the only in situ ionospheric measurements made by MGS came from the magnetometer and electron reflectometer instruments (known together as MAG/ER). Precipitating electrons were confirmed to be an important source of the nightside ionosphere, the patchiness of which is at least partially driven by the presence of crustal magnetic fields that determine which parts of the ionosphere can be accessed by precipitating electrons (e.g., Acuna et al., 1999; Fox, 1993; Haider et al., 1992; Lillis & Fang, 2015; Lillis et al., 2009, 2011; Mitchell et al., 2001; Verigin et al., 1991). The lack of an ion instrument and the ability to measure the cold ionospheric electron population meant that MGS was unable to characterize the cold, bulk ionosphere of Mars with in situ measurements.

The Mars EXpress (MEX) spacecraft reached Mars orbit in late December 2003 and to this date is still operational. MEX carries an Ion Mass Spectrometer (IMA) and an ELectron Spectrometer (ELS), which are part of the Analyzer of Space Plasmas and Energetic Atoms-3 (ASPERA-3) instrument suite (Barabash et al., 2004). IMA has observed energetic ionospheric ions far from Mars, suggesting that energization mechanisms act within the Martian ionosphere that drive ion escape to space (e.g., Dubinin et al., 2006; Dubinin, Modolo, Fraenz, Woch,

Duru, et al., 2008; Dubinin, Modolo, Fraenz, Woch, Chanteur, et al., 2008, Lundin et al., 2004, 2008). The lower energy limit of ASPERA-3 (10 eV) and the relatively long integration time per measurement (196 s) mean that ASPERA-3 is unable to observe small-scale structure and the cold, bulk ionosphere at lower altitudes, but nonetheless has provided exciting glimpses of the physical processes acting within the ionosphere. MEX is able to remotely measure the cold ionospheric electron density with the Mars Advanced Radar for Subsurface and Ionosphere Sounding (MARSIS) instrument, which is a topside radar sounder (Picardi et al., 2004). Echo returns measured by the instrument have shown that the Martian ionosphere is horizontally stratified far from crustal magnetic fields but contains significant structure within these regions (Duru et al., 2006; Gurnett et al., 2005b, 2008). MARSIS measurements have also shown that the dayside ionospheric peak at Mars follows the behavior predicted by Chapman theory (e.g., Fallows et al., 2015a, 2015b; Fox & Yeager, 2006; Liao et al., 2006). The MARSIS measurement technique means that the instrument cannot measure electron densities below a few 10^3 cm^{-3}, and densities below the ionospheric peak are unobtainable.

Radio occultations of the Martian ionosphere have been performed by several missions including the Mars, Mariner, Viking, MGS, and MEX spacecraft (e.g., Fjeldbo et al., 1970; Lindal et al., 1979; Savich and Samovol, 1976). The relative orbital geometries of Earth and Mars mean that radio occultations are only possible at SZA close to the terminator; however, these occultations have shown that the early nighttime ionosphere is highly variable in both overall structure and density and in many cases does not contain a detectable peak in electron density (Zhang et al., 1990). Seasonal effects and structure produced by the crustal magnetic fields have also been observed in radio occultation profiles made by MGS (e.g., Bougher et al., 2004; Breus et al., 2004; Withers et al., 2005). Radio occultation measurements by MEX discovered a third transient layer below the main ionospheric peak whose origin is still not yet fully understood (Crismani et al., 2017; Pätzold et al., 2005).

To summarize, the above missions were capable of sampling large-scale ionospheric structure at Mars, but no one spacecraft could fully characterize all properties of the ionosphere (i.e., neutrals, ions, electrons, and magnetic and electric field). The Mars Atmosphere and Volatile EvolutioN (MAVEN) mission arrived at Mars in late 2014 and is the first dedicated aeronomy mission to Mars that is capable of characterizing these properties, using in situ measurement techniques. The instrumentation on MAVEN confirms many of the observed phenomenon reported by previous missions and allows for the investigation of smaller-scale features in the ionosphere. This paper presents observations of small-scale, highly structured electron densities in the lower Martian ionosphere that occur preferentially near the Martian terminator (defined here as roughly 80° < SZA <120°). These observations are evocative of ionospheric irregularities observed in the terrestrial *E* region, although more detailed analysis and modeling are necessary to conclusively determine the causes of the observed irregularities at Mars. The data analyzed in this study are described in section 2, and a single event is analyzed in section 3. A statistical study of similar events is shown in section 4. We discuss our observations in section 5 before concluding in section 6.

2. Data

The MAVEN spacecraft is a dedicated aeronomy mission with the primary science goals of understanding the physical processes that act within the Martian upper atmosphere and to evaluate how the Martian atmosphere has evolved over time (Jakosky et al., 2015). This study utilizes data from several instruments on board MAVEN, namely, the Langmuir Probe and Waves (LPW) (Andersson et al., 2014), the fluxgate magnetometer (MAG) (Connerney et al., 2015), the Neutral Gas and Ion Mass Spectrometer (NGIMS) (Benna et al., 2015; Mahaffy, Benna, Elrod, et al., 2015; Mahaffy, Benna, King, et al., 2015), and the Solar Wind Electron Analyzer (SWEA) (Mitchell et al., 2016) instruments.

LPW consists of two ~7 m booms separated by an angular distance of ~110°. Current-voltage (I-V) characteristics are measured at a cadence of 1 s for the data presented here. Due to the instrument mode of operation, I-V characteristics were measured for the first 3 s out of every 4; an I-V characteristic was not measured on the fourth second. The local electron density (N_e), electron temperature (T_e), and spacecraft potential (V_{sc}) are derived by analysis of individual measured I-V characteristics and are thus available at matching cadences (Ergun et al., 2015). MAG measures the vector magnetic field at a rate of 32 Hz. NGIMS is able to measure multiple mass to charge ratios in quick succession and is able to measure most neutral and ion species during the same periapsis pass. The measurement cadence for any species is typically around 2.6 s but can vary depending on the number of species being measured on any given periapsis pass. SWEA is a hemispherical

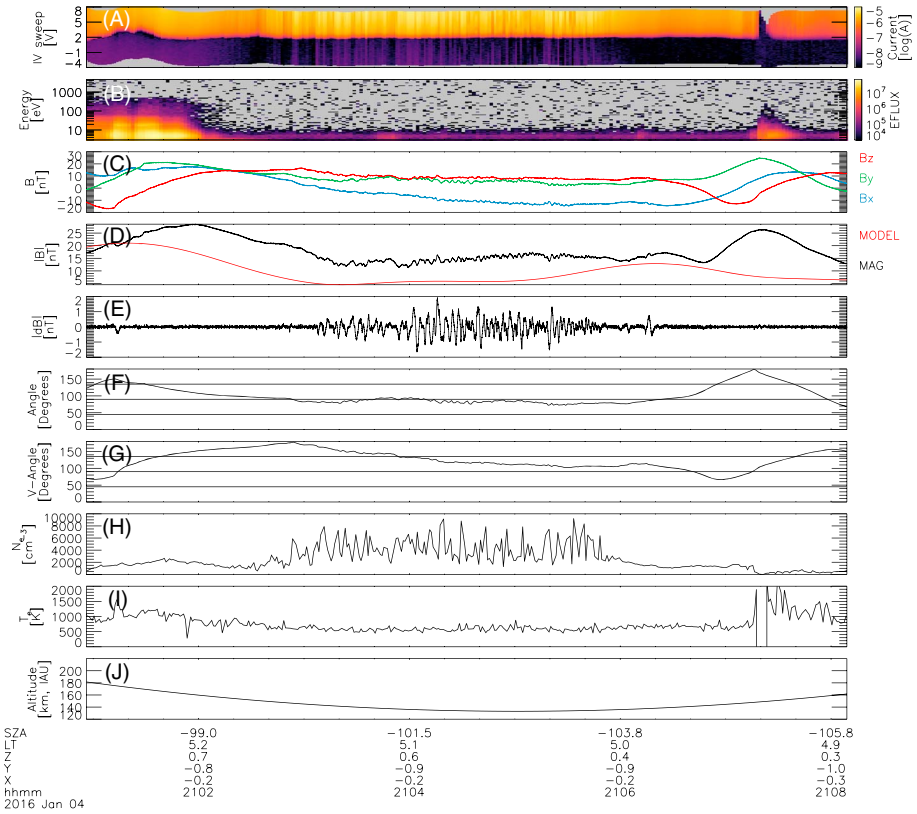

Figure 1. Time series plasma data for the studied event. (a) LPW I-V characteristics. (b) SWEA suprathermal electron energy flux. (c) The 3-D magnetic field in the MSO frame. (d) Total magnetic field strength (black) and modeled crustal magnetic fields (red) (Morschhauser et al., 2014). (e) High-frequency variation in magnetic field. (f) Angle between magnetic field and vertical direction. (g) Angle between magnetic field and spacecraft velocity vector. (h) N_e. (i) T_e. (j) Altitude in the IAU-Mars frame. The fluctuations in magnetic field and electron density mark the region of interest, between 21:03:00 and 21:05:30 UTC.

electrostatic analyzer that measures electron fluxes from 3 eV up to 5 keV. It has a 360°×120° field of view provided by electrostatic deflectors and a time resolution of 2 s. The data version (V) and revision (R) numbers used in this study (where applicable) are as follows: LPW: V2, R1; NGIMS: V6, R2; and SWEA: V3, R3.

3. Event

MAVEN has observed the ionospheric irregularities reported in this study below 200 km in altitude. Quasiperiodic fluctuations in magnetic field and ionospheric density are observed spanning ~10 s up to several minutes in time series data. Time series plasma data of such event are shown in Figure 1; periapsis location for this orbit was at the predawn equatorial terminator at approximately 4 January 2016/21:05 UTC. Figure 1a shows the LPW I-V characteristics; the SWEA suprathermal electron energy flux is shown in Figure 1b; the 3-D magnetic field in Mars Solar Orbital (MSO) coordinates is shown in Figure 1c; the magnitude of the 3-D magnetic field is the black line in Figure 1d, and the modeled crustal magnetic field strength is the red line in Figure 1d (Acuna et al., 1999; Morschhauser et al., 2014). The MSO frame is orthogonal, defined as positive *X* pointing along the Mars-Sun line, toward the Sun; *Y* points approximately opposite to Mars' orbital motion, and *Z* is perpendicular to Mars' orbital plane. The high-frequency ($\gtrsim$0.1 Hz) variation in the total magnetic field strength (black line, Figure 1d) is shown in Figure 1e. The angle between the local 3-D magnetic field and the vertical direction is shown in Figure 1f; values of 0° and 180° denote upward and downward pointing field, respectively; 90° signifies magnetic field horizontal to the planet's surface. The angle between the 3-D magnetic field vector and the spacecraft velocity vector is shown in Figure 1g. Values of 0° and 180° mean that MAVEN is traveling parallel to the local magnetic field; 90° means that MAVEN is traveling perpendicular to the local magnetic field. Horizontal guide lines have been added at 45°, 90° and 135° to Figures 1f and 1g for clarity. The local N_e and T_e are shown in Figures 1h and 1i, respectively. The spacecraft altitude in the International

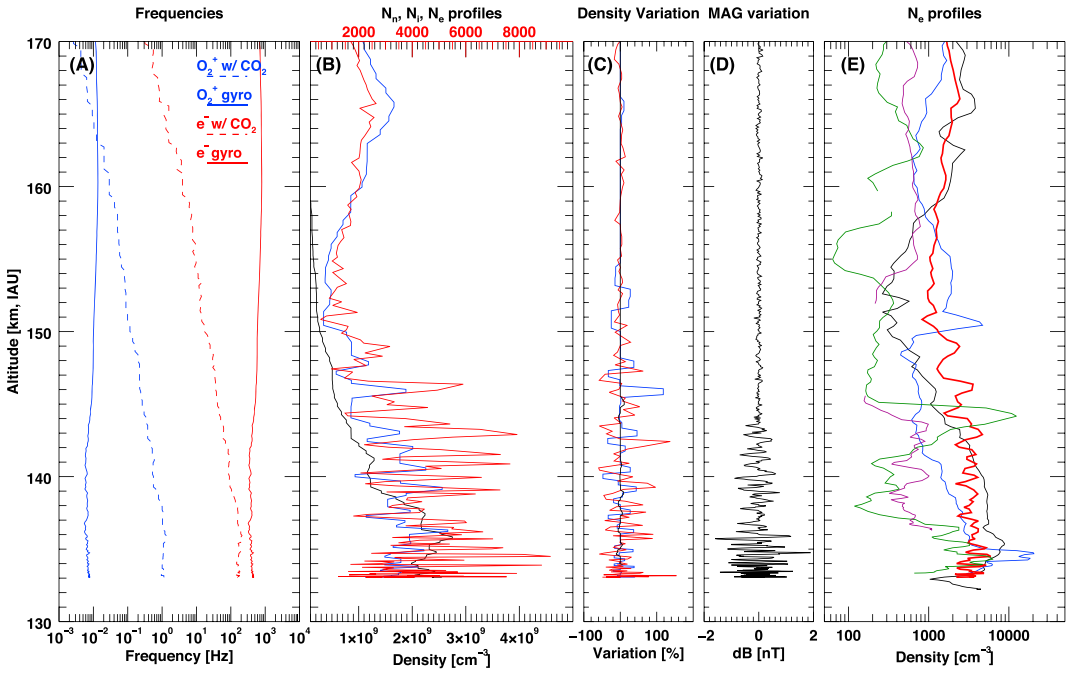

Figure 2. Various parameters for the inbound segment of the orbit shown in Figure 1. (a) Collision and gyrofrequencies for the species labeled in the plot. (b) Neutral CO_2 density (black, bottom axis) and ion and electron density (blue and red, respectively, top axis). (c) The percentage variation of the species shown in Figure 2b. (d) The high-frequency variation in magnetic field. (e) N_e for this event (red); N_e for neighboring orbits where irregularities were not present (lighter colors).

Astronomical Union Mars planetodetic (IAU-Mars) reference frame is shown in Figure 1j. The SZA, local time, and position coordinates in the MSO frame are printed underneath the bottom panel, in units of degrees, hour, and Mars radii, respectively. Negative SZA denote dawn, positive dusk. Quasiperiodic fluctuations in magnetic field and plasma density that are the subject of this study occur below about 150 km, between approximately 21:03:00 and 21:05:30 UTC.

Various parameters for the inbound segment of this event are shown in Figure 2 as a function of altitude. The majority of the event was observed on the inbound portion of the orbit, and therefore, we do not show the outbound segment here. CO_2 and O_2^+ were the dominant neutral and ion species below about 165 km and 180 km, respectively, and the corresponding density profiles for these species are shown as the black and blue lines, respectively, in Figure 2b. The red line shows electron density; the blue and red lines are referenced to the top *x* axis scale. The percentage variation of these three profiles is shown in Figure 2c, where the colors match those in Figure 2b.

Figure 2a shows the collision frequencies (Schunk & Nagy, 2009) of O_2^+ and electrons, with neutral CO_2, in dashed blue and red, respectively. Corresponding gyrofrequencies for O_2^+ and electrons about the local magnetic field are shown in solid blue and red, respectively, in the same panel. The electron gyrofrequency is always at least a factor of ~3–4 greater than the electron CO_2 collision frequency, and as such the electrons are mostly magnetized throughout the entire periapsis pass. O_2^+, on the other hand, is unmagnetized below about ~163 km. The ion and electron density profiles in Figure 2b show similar variations across all altitudes and exhibit large fluctuations across small (a few kilometers) altitude ranges when the fluctuations in magnetic field are present. These density fluctuations are ~50% for O_2^+ and up to almost 200% for the electrons (Figure 2c). In contrast, the neutral CO_2 density profile shows very little variation, <10%. Differences between ion and electron densities are at least in part due to differences in measurement cadence and integration time: NGIMS density measurements for a single species are taken over several tens of milliseconds, while the LPW I-V characteristics were measured over 1 s.

The variation in magnetic field is shown in Figure 2d; this is the same data as shown in Figure 1d. Close inspection of the data showed a strong, but not perfect, correlation between peaks in electron density and peaks

in magnetic field strength (not shown here). The imperfect correlation may be because the ion and electron measurements undersample the observed variations due to their lower sampling rates, compared to the MAG instrument.

The quasiperiodic variations in magnetic field (which are at about 0.1 Hz) are clearly visible in Figures 1c, 1d (21:03:00 to 21:05:30 UTC), and 2d and are of the order of 1–3 nT in amplitude (Figure 1e). The magnetic field is horizontal during the event (Figure 1f) and appears to contain very little contribution from the localized crustal magnetic fields (although the Morschhauser crustal field model is not well constrained at these low altitudes and may contain errors of 5–10 nT). Stronger crustal magnetic fields are observed before ~21:02:40 UTC and after ~21:06:30 UTC, and the fluctuations in magnetic field are not present during such times.

The large variations in plasma density are clearly visible in both the LPW and NGIMS plasma density data (Figures 1h and 2b). These fluctuations are also clearly present in the measured I-V characteristics from LPW, confirming that these variations in electron density are real and not a result of poor fitting during analysis of the I-V characteristics for this event. The mainly horizontal motion of the spacecraft and collisional nature of the atmosphere (Figure 2a) at periapsis means that these density (and corresponding magnetic) fluctuations are likely standing structures; when Doppler shift is taken into account due to the spacecraft motion (~4 km s^{-1} at periapsis), these fluctuations have length scales of 15–20 km. There is no significant variation in electron temperature (Figure 1i), suggesting that the same plasma population is present throughout the event. Large, unstable values of spacecraft potential can degrade ion and electron plasma measurements; the spacecraft potential was essentially constant throughout this periapsis pass at a value of ~ -2 V.

Electrons measured by SWEA in Figure 1b are produced from photoionization of the neutral atmosphere; the observed lack of significant energy flux after ~21:02 UTC suggests a lack of photoionizing light at such times, which is expected as the spacecraft is past the EUV terminator. The small patch of suprathermal electrons observed on the outbound portion of the orbit, just after 21:07 UTC in Figure 1b, is most likely precipitating electrons. These are a known source of the Martian nightside ionosphere and are not discussed further here (e.g., Fowler et al., 2015; Fox, 1993; Haider et al., 1992; Lillis and Fang, 2015; Lillis et al., 2011, 2009; Verigin et al., 1991).

The electron density profile for this event is shown as the red line in Figure 2e. The black, blue, green, and purple lines show electron density profiles from four neighboring orbits where ionospheric irregularities were not observed and are included as a reference as to how normal density variations can appear for this location. The electron density profile for this event (red) does not stand out from the neighboring passes; all five density profiles show large variability due to the terminator location of periapsis.

4. Statistical Study

Events similar to those shown in Figure 1 were identified from 31 months of MAVEN data, spanning November 2014 through May 2017, below altitudes of 200 km. Events were identified when the standard deviation (across a 3 s sliding window) of the variation in magnetic field strength (Figure 1e) was greater than 0.1 nT, for at least 20 s. The 20 s time constraint reduces false detections produced from sudden changes in magnetic field strength that are associated with crustal magnetic fields and field-aligned currents.

Ionospheric irregularities were identified on 179 MAVEN orbits using an automated routine. The normalized distribution of these events with respect to SZA is shown by the black line in Figure 3a (i.e., the black line shows the fraction (number of separate orbits where at least one event was observed for this SZA bin)/(the total number of separate orbits that passed through this SZA bin)). Negative SZA are dawn; positive dusk; 0° is noon and ±180° is midnight. The black line has thus been normalized by the red line, which shows the total number of orbits that sampled each SZA bin. This accounts for the fact that few measurements currently exist at the subsolar point and close to midnight. The black error bars are the statistical $\sqrt{N}$ errors, where N is the number of detected events in each SZA bin. There are clear peaks in occurrence just past the dawn and dusk terminators, at ~±(90° to 110°). The peaks in occurrence at small |SZA| are partly a result of low number statistics; three orbits, all from 23 April 2015 UTC, comprise the spike at −10° to 0° SZA. The outbound density profiles for these orbits are shown as the colored lines in Figure 3c. The gray dots show density profiles from 6 days either side of this UTC day. The colored profiles show significantly more variation, and reduced densities, than the majority of the gray orbits. The close to noon location is an unexpected location to observe such

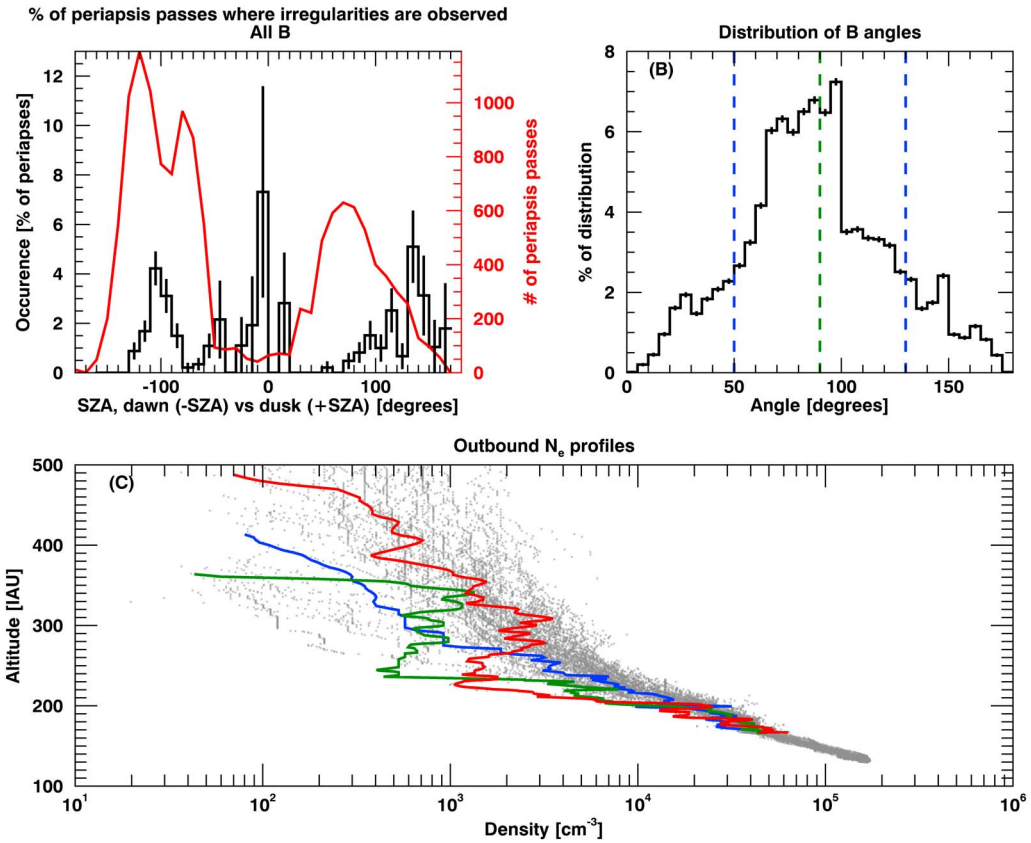

Figure 3. Statistical analysis of events similar to those shown in Figure 1, identified by variations in magnetic field strength. (a) The normalized distribution of events (black) and the total number of orbit samples (red) as functions of SZA. (b) The distribution of magnetic field angles for the events shown by the black line in Figure 3a; 90° is horizontal and 0° and 180° are vertical field. (c) N_e profiles for the three events that comprise the spike in occurrence at −10° to 0° in the black line in Figure 3a (colored lines). The gray dots show density profiles for ~25 orbits either side of these events.

drastic variation in electron density, and more measurements are required before the importance of these highly variable profiles can be quantified.

The distribution of magnetic field angles relative to the local horizontal throughout the 179 identified events is shown in Figure 3b. The vertical green line marks horizontal field; the two blue lines enclose 75% of the distribution. The error bars are again $\sqrt{N}$.

5. Discussion

At first glance, conditions below 200 km in the Martian ionosphere appear comparable to the terrestrial *E* region. The major ion species are unmagnetized because $\nu_{in} \gg \Omega_{ci}$ and their motion is governed by the neutral atmosphere, while electrons are magnetized. Here ν_{in} is the ion-neutral collision frequency, and Ω_{ci} is the ion cyclotron frequency. At the terminator (~80° < SZA < 120°), a lack of photoionizing light results in the ionospheric peak rising in altitude, leading to an ionospheric plasma density gradient pointing upward at low altitudes. The ionospheric peak at the terminator is located, on average, at around 180 km (Fowler et al., 2015), compared to ~125 km at the subsolar point (e.g., Ergun et al., 2015; Gurnett et al., 2005a; Morgan et al., 2008; Nielsen et al., 2007).

Ionospheric irregularities have been extensively studied in the terrestrial *E* region and are characterized by highly variable ionospheric densities and electric fields (e.g., Brace et al., 1973; Berkner & Wells, 1937; Bettinger, 1965; Chen et al., 1965; Evans, 1969; Farley, 1971; Prakash et al., 1972; Smith and Klaus, 1978). The events presented in this study share several characteristics with irregularities observed at Earth and also exhibit several interesting differences. Irregularities at Earth are typically driven by a modified two-stream instability

(known as the Farley-Buneman instability) or the gradient drift instability (e.g., Balsley, 1969; Basu, 2005; Buneman, 1963; Cohen & Bowles, 1967; Farley, 1963; Fejer & Kelley, 1980; Oppenheim, 1997). These are electrostatic instabilities that lead to irregularities on kilometer scales or less. The electrostatic nature of these waves is justified, in part, because the Earth's ionosphere is a low β plasma ($\beta \lesssim 10^{-4}$, where $\beta = 8\pi nkT/B^2$).

However, the Martian ionosphere is not a low β plasma. For example, for $n \approx 5 \times 10^3$ cm^{-3}, $T \approx 0.1$ eV, and $B \approx 15$ nT, we find $\beta \approx 1$. Thus, the plasma and magnetic pressures are comparable and we would expect irregularities to develop in both the electron density and magnetic field as observed in the data. The irregularities presented in Figure 1 have apparent length scales of ~15–20 km, based on the quasiperiodic fluctuations observed in electron density and magnetic field strength, with a (mostly horizontal) spacecraft velocity of ~4 km s^{-1}. The 1 s integration time for a single LPW I-V sweep means, however, that these irregularities are not fully resolved in electron density. Electromagnetic Farley-Buneman waves have been predicted to exist in the solar atmosphere (Liperovsky et al., 2000) but, to our knowledge, have not been reported elsewhere, and it is unclear whether the irregularities presented here are such waves or not.

The apparent larger length scales and electromagnetic nature of the irregularities observed here make it unclear as to the physical mechanisms acting to produce them. Knowledge of the neutral wind vectors (that would drive ion winds in the collisional regime) relative to the local magnetic field would aid in the interpretation of these events. Neutral wind measurements made by the NGIMS instrument on MAVEN began in 2016 and are made on an approximately monthly basis (because neutral and ion density measurements cannot be made simultaneously with these wind measurements) and exist at cadences of several tens of seconds.

The Suprathermal and Thermal Ion Composition instrument (STATIC) (McFadden et al., 2015) on board MAVEN is able to determine the direction of ion flows, but such data products are currently undergoing calibration. The verification of any flows (neutral or ion) associated with these irregularities is thus difficult at this time.

In the terrestrial equatorial ionosphere, vertical electric fields can drive and enhance ionospheric irregularities. Several drivers of electric field exist in the terrestrial ionosphere, including neutral winds, conductivity structure, and externally mapped electric fields. Such sources likely exist at Mars; however, a lack of 3-D electric field measurements at Mars (by any mission) makes this difficult to determine. The LPW instrument on MAVEN is able to make 1-D electric field measurements; however, a change in instrument operation mode means that these measurements have not been made since mid-December 2015. Thus, coincident neutral wind and electric field measurements are unavailable on MAVEN, and neither measurement was made during the event shown in Figure 1. Global thermospheric models can provide first-order neutral wind velocity vectors but do not currently provide large-scale electric field vectors in the lower ionosphere (S. Bougher, private communication, 2017).

A further interesting difference between the terrestrial and Martian environments is the large-scale magnetic field topology. Earth possesses, to first order, a dipole magnetic field such that the local magnetic field is horizontal and pointing in a meridional direction at the equatorial terminator. Mars does not possess a significant dipole magnetic field, and the solar wind magnetic field subsequently drapes around the planet so that the large-scale field is horizontal and tailward pointing at the terminator (Bertucci et al., 2004). Global thermospheric models predict zonal winds at the Martian terminator of 100–200 ms^{-1} at 200 km altitude (Bougher et al., 2015), and these models are currently being validated with MAVEN data. It is unclear how the large-scale draped magnetic field topology at Mars effects the generation of electric fields in the ionosphere.

The distribution of magnetic field angles during the 179 identified events (Figure 3b) shows that horizontal field is the most likely orientation during such irregularities, as is expected under draped magnetic field conditions at the terminator. The statistical distribution of these events as a function of SZA (Figure 3a) shows that such irregularities are most likely to be observed just past the Martian terminator (SZA ~ ±(90° to 110°)). There is, however, a significant asymmetry between the dawn and dusk terminator, where irregularities are observed well into the night on the duskside. Such an asymmetry may be in part a result of asymmetric ionospheric densities premidnight and postmidnight, which were reported by Fowler et al. (2015). The few events observed close to the subsolar point in Figure 3a occur under highly disturbed ionospheric conditions. These orbits are shown as the colored lines in Figure 3c; note that a wider altitude range is shown here, demonstrating the highly disturbed ionosphere across all altitudes for these cases. MAVEN cannot sample the solar wind, while periapsis is close to the subsolar point, but the reduced ionospheric densities above

~300 km altitude suggest that upstream conditions are driving the dayside ionosphere for these orbits. The highly variable profiles provide small regions of vertical density gradient that do not typically occur at these SZA; solar EUV can reach well below 130 km altitude here to provide ionization (e.g., Ergun et al., 2015; Gurnett et al., 2005a; Němec et al., 2011). Ionospheric irregularities could thus be common at the subsolar region despite these EUV conditions, but more observations are required to confirm this.

Interestingly, unusual (and yet unexplained) wave phenomena was observed by the Pioneer Venus Orbiter satellite downstream of the terminator (Brace et al., 1983). Large-scale fluctuations ($\lambda \sim 150$ km) in the electron density and temperature, as well as magnetic field, were observed below 200 km. These irregularities occur in a region of the ionosphere where the ions are unmagnetized and the electrons are magnetized, similar to the situation reported here. Additionally, smaller-scale electron density fluctuations ($\lambda \sim 0.1-2.0$ km) were also observed under these conditions but in the nightside Venus ionosphere (Grebowsky et al., 1991). These waves were attributed to the lower-hybrid-drift instability (Huba, 1992; Huba & Grebowsky, 1993). Although the wavelengths observed by Brace et al. (1983) at Venus are much greater than those observed at Mars, and those observed by Grebowsky et al. (1991) are somewhat shorter, the similarities of the conditions may suggest common mechanisms to generate these irregularities.

6. Conclusions

Ionospheric irregularities have been observed below 200 km altitude in the Martian ionosphere that are characterized by large, quasiperiodic fluctuations in plasma density and magnetic field strength. At such low altitudes, the Martian ionosphere is similar to the terrestrial *E* region and the lower portion of the Venusian ionosphere, in that the ions are unmagnetized while the electrons are magnetized.

Several properties of the irregularities observed at Mars are unlike irregularities observed in the terrestrial ionosphere. The irregularities reported here appear to be electromagnetic in nature, in contrast to the electrostatic nature of irregularities at Earth. The event presented here (Figure 1) exhibits length scales of 15–20 km, which are larger than typical length scales of irregularities at Earth that tend to be a kilometer or less.

The global, draped, magnetic field topology at Mars differs substantially from the dipole nature of the field at Earth. The magnetic field at the Martian terminator is to first order aligned with the expected neutral winds at low altitudes, and it is unclear how this affects the generation of vertical electric fields, as occurs within the terrestrial dynamo region at the equatorial terminator. The lack of 3-D electric field measurements by MAVEN makes it difficult to investigate the structure and drivers of electric fields in the Martian ionosphere.

It is clear that the observed irregularities are an important feature of the low-altitude Martian ionosphere, but a conclusive description of how they form is not yet clear. A more apt comparison for future work is probably the Venusian ionosphere, given the lack of a strong global dipole magnetic field there, as opposed to Earth.

Acknowledgments
Work at LASP and SSL was supported by NASA funding for the MAVEN project through the Mars Exploration Program. Data used in this study are available on the NASA Planetary Data System, via https://pds.nasa.gov/. We thank the anonymous reviewers for taking the time and effort to review this manuscript and helping to improve it through the peer review process.

References

Acuna, M., Connerney, J., Lin, R., Mitchell, D., Carlson, C., McFadden, J., … Cloutier, P. (1999). Global distribution of crustal magnetization discovered by the Mars Global Surveyor MAG/ER experiment. *Science*, *284*(5415), 790–793.

Andersson, L., Ergun, R. E., Delory, G. T., Eriksson, A., Westfall, J., Reed, H., … Meyers, D. (2014). The Langmuir Probe and Waves (LPW) instrument for MAVEN. *Space Science Reviews*, *195*, 173–198.

Balsley, B. B. (1969). Some characteristics of non-two-stream irregularities in the equatorial electrojet. In *frequency waves and irregularities in the ionosphere: Proceedings of the 2nd Esrin-Eslab Symposium, Held in Frascati, Italy, 23–27 September, 1968* (pp. 152–172). Dordrecht, Netherlands: Springer. https://doi.org/10.1007/978-94-010-3402-9_12

Barabash, S., Lundin, R., Andersson, H., Gimholt, J., Holmström, M., Norberg, O., … Bochsler, P. (2004). ASPERA-3: Analyser of space plasmas and energetic ions for Mars Express. In A. Wilson (Ed.), *Mars Express: The scientific payload* (Vol. 1240, pp. 121–139). Noordwijk, Netherlands: ESA Publications Division.

Basu, B. (2005). Characteristics of electromagnetic Rayleigh-Taylor modes in nighttime equatorial plasma. *Journal of Geophysical Research*, *110*, A02303. https://doi.org/10.1029/2004JA010659

Benna, M., Mahaffy, P., Grebowsky, J., Fox, J. L., Yelle, R. V., & Jakosky, B. M. (2015). First measurements of composition and dynamics of the Martian ionosphere by MAVEN's neutral gas and ion mass spectrometer. *Geophysical Research Letters*, *42*, 8958–8965. https://doi.org/10.1002/2015GL066146

Berkner, L. V., & Wells, H. W. (1937). Abnormal ionization of the *E*-region of the ionosphere. *Terrestrial Magnetism and Atmospheric Electricity (Journal of Geophysical Research)*, *42*, 73–76. https://doi.org/10.1029/TE042i001p00073

Bertucci, C., Mazelle, C., Crider, D. H., Mitchell, D. L., Sauer, K., Acuña, M. H., … Winterhalter, D. (2004). MGS MAG/ER observations at the magnetic pileup boundary of Mars: Draping enhancement and low frequency waves. *Advances in Space Research*, *33*(11), 1938–1944.

Bettinger, R. (1965). An in situ probe system for measurement of ionospheric parameters. In F. Singer (Ed.), *Interactions of space vehicles with an ionized atmosphere*. London: Pergamon Press.

Bougher, S. W., Engel, S., Hinson, D. P., & Murphy, J. R. (2004). MGS Radio Science electron density profiles: Interannual variability and implications for the Martian neutral atmosphere. *Journal of Geophysical Research*, *109*, E03010. https://doi.org/10.1029/2003JE002154

Bougher, S., Pawlowski, D., Bell, J., Nelli, S., McDunn, T., Murphy, J., … Ridley, A. (2015). Mars Global Ionosphere-Thermosphere Model: Solar cycle, seasonal, and diurnal variations of the Mars upper atmosphere. *Journal of Geophysical Research: Planets*, *120*, 311–342. https://doi.org/10.1002/2014JE004715

Brace, L., Theis, R., & Dalgarno, A. (1973). The cylindrical electrostatic probes for Atmosphere Explorer-C, -D, and -E. *Radio Science*, *8*(4), 341–348.

Brace, L., Elphic, R., Curtis, S., & Russell, C. (1983). Wave structure in the Venus ionosphere downstream of the terminator. *Geophysical Research Letters*, *10*(11), 1116–1119.

Breus, T. K., Krymskii, A. M., Crider, D. H., Ness, N. F., Hinson, D., & Barashyan, K. K. (2004). Effect of the solar radiation in the topside atmosphere/ionosphere of Mars: Mars Global Surveyor observations. *Journal of Geophysical Research*, *109*, A09310. https://doi.org/10.1029/2004JA010431

Buneman, O. (1963). Excitation of field aligned sound waves by electron streams. *Physical Review Letters*, *10*(7), 285–287.

Chen, F. F. (1965). Electric probes. In R. H. Huddlestone & S. L. Leornard (Eds.), *Plasma diagnostic techniques* (pp. 113–200). New York: Academic Press.

Cohen, R., & Bowles, K. L. (1967). Secondary irregularities in the equatorial electrojet. *Journal of Geophysical Research*, *72*(3), 885–894.

Connerney, J. E. P., Espley, J., Lawton, P., Murphy, S., Odom, J., Oliversen, R., & Sheppard, D. (2015). The MAVEN magnetic field investigation. *Space Science Reviews*, *195*(1–4), 257–291. https://doi.org/10.1007/s11214-015-0169-4

Crismani, M. M., Schneider, N. M., Plane, J. M., Evans, J. S., Jain, S. K., Chaffin, M. S., … Jakosky, B. M. (2017). Detection of a persistent meteoric metal layer in the Martian atmosphere. *Nature Geoscience*, *10*(6), 401–404.

Dubinin, E., Lundin, R., Fraenz, M., Woch, J., Barabash, S., Fedorov, A., … Carter, M. (2006). Electric fields within the Martian magnetosphere and ion extraction: ASPERA-3 observations. *Icarus*, *182*(2), 337–342.

Dubinin, E., Modolo, R., Fraenz, M., Woch, J., Duru, F., Akalin, F., … Picardi, G. (2008). Structure and dynamics of the solar wind/ionosphere interface on Mars: MEX-ASPERA-3 and MEX-MARSIS observations. *Geophysical Research Letters*, *35*, L11103. https://doi.org/10.1029/2008GL033730

Dubinin, E., Modolo, R., Fraenz, M., Woch, J., Chanteur, G., Duru, F., … Picardi, G. (2008). Plasma environment of Mars as observed by simultaneous MEX-ASPERA-3 and MEX-MARSIS observations. *Journal of Geophysical Research*, *113*, A10217. https://doi.org/10.1029/2008JA013355

Duru, F., Gurnett, D. A., Averkamp, T. F., Kirchner, D. L., Huff, R. L., Persoon, A. M., … Picardi, G. (2006). Magnetically controlled structures in the ionosphere of Mars. *Journal of Geophysical Research*, *111*, A12204. https://doi.org/10.1029/2006JA011975

Ergun, R., Morooka, M., Andersson, L., Fowler, C., Delory, G., Andrews, D., … Jakosky, B. (2015). Dayside electron temperature and density profiles at Mars: First results from the MAVEN Langmuir Probe and Waves instrument. *Geophysical Research Letters*, *42*, 8846–8853. https://doi.org/10.1002/2015GL065280

Evans, J. (1969). Theory and practice of ionosphere study by Thomson scatter radar. *Proceedings of the IEEE*, *57*(4), 496–530.

Fallows, K., Withers, P., & Matta, M. (2015a). An observational study of the influence of solar zenith angle on properties of the M1 layer of the Mars ionosphere. *Journal of Geophysical Research: Space Physics*, *120*, 1299–1310. https://doi.org/10.1002/2014JA020750

Fallows, K., Withers, P., & Matta, M. (2015b). Numerical simulations of the influence of solar zenith angle on properties of the M1 layer of the Mars ionosphere. *Journal of Geophysical Research: Space Physics*, *120*, 6707–6721. https://doi.org/10.1002/2014JA020947

Farley, D. (1971). Radio wave scattering from the ionosphere. *Methods in Experimental Physics*, *9*, 139–186.

Farley, D. (1963). Two-stream plasma instability as a source of irregularities in the ionosphere. *Physical Review Letters*, *10*(7), 279.

Fejer, B. G., & Kelley, M. (1980). Ionospheric irregularities. *Reviews of Geophysics*, *18*(2), 401–454.

Fjeldbo, G., Kliore, A., & Seidel, B. (1970). The Mariner 1969 occultation measurements of the upper atmosphere of Mars. *Radio Science*, *5*(2), 381–386.

Fowler, C., Andersson, L., Ergun, R., Morooka, M., Delory, G., Andrews, D. J., … Jakosky, B. M. (2015). The first in situ electron temperature and density measurements of the Martian nightside ionosphere. *Geophysical Research Letters*, *42*, 8854–8861. https://doi.org/10.1002/2015GL065267

Fox, J. L. (1993). Upper limits to the nightside ionosphere of Mars. *Geophysical Research Letters*, *20*(13), 1339–1342.

Fox, J. L., & Yeager, K. E. (2006). Morphology of the near-terminator Martian ionosphere: A comparison of models and data. *Journal of Geophysical Research*, *111*, A10309. https://doi.org/10.1029/2006JA011697

Grebowsky, J., Curtis, S., & Brace, L. (1991). Small-scale plasma irregularities in the nightside Venus ionosphere. *Journal of Geophysical Research*, *96*(A12), 21,347–21,359.

Gurnett, D., Huff, R., Morgan, D., Persoon, A., Averkamp, T., Kirchner, D., … Picardi, G. (2008). An overview of radar soundings of the Martian ionosphere from the Mars Express spacecraft. *Advances in Space Research*, *41*(9), 1335–1346.

Gurnett, D., Kirchner, D., Huff, R., Morgan, D., Persoon, A., Averkamp, T., … Picardi, G. (2005a). Radar soundings of the ionosphere of Mars. *Science*, *310*(5756), 1929–1933.

Gurnett, D. A., Kirchner, D. L., Huff, R. L., Morgan, D. D., Persoon, A. M., Averkamp, T. F., … Picardi, G. (2005b). Radar soundings of the ionosphere of Mars. *Science*, *310*(5756), 1929–1933. https://doi.org/10.1126/science.1121868

Haider, S., Kim, J., Nagy, A., Keller, C., Verigin, M., Gringauz, K., … Kiraly, P. (1992). Calculated ionization rates, ion densities, and airglow emission rates due to precipitating electrons in the nightside ionosphere of Mars. *Journal of Geophysical Research*, *97*(A7), 10,637–10,641.

Hanson, W., Sanatani, S., & Zuccaro, D. (1977). The Martian ionosphere as observed by the Viking retarding potential analyzers. *Journal of Geophysical Research*, *82*(28), 4351–4363.

Huba, J. (1992). Theory of small-scale density and electric field fluctuations in the nightside Venus ionosphere. *Journal of Geophysical Research*, *97*(A1), 43–50.

Huba, J., & Grebowsky, J. (1993). Small-scale density irregularities in the nightside Venus ionosphere: Comparison of theory and observations. *Journal of Geophysical Research*, *98*(E2), 3079–3086.

Jakosky, B. M., Lin, R. P., Grebowsky, J. M., Luhmann, J. G., Mitchell, D. F., Beutelschies, G., … Zurek, R. (2015). The Mars Atmosphere and Volatile EvolutioN (MAVEN) mission. *Space Science Reviews*, *195*, 1–46.

Liao, H.-R., Wang, J.-S., Zou, H., & Wang, X.-D. (2006). Observational features of the secondary layer of the Martian ionosphere. *Advances in Geosciences*, *3*, 135–143.

Lillis, R. J., & Fang, X. (2015). Electron impact ionization in the Martian atmosphere: Interplay between scattering and crustal magnetic field effects. *Journal of Geophysical Research*, *120*, 1332–1345. https://doi.org/10.1002/2015JE004841

Lillis, R. J., Fillingim, M. O., & Brain, D. A. (2011). Three-dimensional structure of the Martian nightside ionosphere: Predicted rates of impact ionization from Mars Global Surveyor magnetometer and electron reflectometer measurements of precipitating electrons. *Journal of Geophysical Research*, *116*, A12317. https://doi.org/10.1029/2011JA016982

Lillis, R. J., Fillingim, M. O., Peticolas, L. M., Brain, D. A., Lin, R. P., & Bougher, S. W. (2009). Nightside ionosphere of Mars: Modeling the effects of crustal magnetic fields and electron pitch angle distributions on electron impact ionization. *Journal of Geophysical Research*, *114*, E11009. https://doi.org/10.1029/2009JE003379

Lindal, G. F., Hotz, H. B., Sweetnam, D. N., Shippony, Z., Brenkle, J. P., Hartsell, G. V., … Michael, W. H. (1979). Viking radio occultation measurements of the atmosphere and topography of Mars: Data acquired during 1 Martian year of tracking. *Journal of Geophysical Research*, *84*(B14), 8443–8456.

Liperovsky, V., Meister, C.-V., Liperovskaya, E., Popov, K., & Senchenkov, S. (2000). On the generation of modified low-frequency Farley-Buneman waves in the solar atmosphere. *Astronomische Nachrichten*, *321*(2), 129–136.

Lundin, R., Barabash, S., Andersson, H., Hölmstrom, M., Grigoriev, A., Yamauchi, M., & Bochsler, P. (2004). Solar wind-induced atmospheric erosion at Mars: First results from ASPERA-3 on Mars Express. *Science*, *305*(5692), 1933–1936. https://doi.org/10.1126/science.1101860

Lundin, R., Barabash, S., Hölmstrom, M., Nilsson, H., Yamauchi, M., Fraenz, M., & Dubinin, E. M. (2008). A comet-like escape of ionospheric plasma from Mars. *Geophysical Research Letters*, *35*, L18203. https://doi.org/10.1029/2008GL034811

Mahaffy, P., Benna, M., Elrod, M., Yelle, R., Bougher, S., Stone, S., & Jakosky, B. (2015). Structure and composition of the neutral upper atmosphere of Mars from the MAVEN NGIMS investigation. *Geophysical Research Letters*, *42*, 8951–8957. https://doi.org/10.1002/2015GL065329

Mahaffy, P. R., Benna, M., King, T., Harpold, D. N., Arvey, R., Barciniak, M., … Nolan, J. T. (2015). The neutral gas and ion mass spectrometer on the Mars Atmosphere and Volatile EvolutioN mission. *Space Science Reviews*, *195*(1-4), 49–73.

McFadden, J. P., Kortmann, O., Curtis, D., Dalton, G., Johnson, G., Abiad, R., … Jakosky, B. (2015). MAVEN Suprathermal and Thermal Ion Composition (STATIC) instrument. *Space Science Reviews*, *195*(1), 199–256. https://doi.org/10.1007/s11214-015-0175-6

Mitchell, D., Lin, R., Mazelle, C., Reme, H., Cloutier, P., Connerney, J., … Ness, N. (2001). Probing Mars' crustal magnetic field and ionosphere with the MGS Electron Reflectometer. *Journal of Geophysical Research*, *106*(E10), 23,419–23,427.

Mitchell, D. L., Mazelle, C., Sauvaud, J.-A., Thocaven, J.-J., Rouzaud, J., Fedorov, A., … Jakosky, B. M. (2016). The MAVEN solar wind electron analyzer. *Space Science Reviews*, *200*(1), 495–528. https://doi.org/10.1007/s11214-015-0232-1

Morgan, D., Gurnett, D., Kirchner, D., Fox, J. L., Nielsen, E., & Plaut, J. (2008). Variation of the Martian ionospheric electron density from Mars Express radar soundings. *Journal of Geophysical Research*, *113*, A09303. https://doi.org/10.1029/2008JA013313

Morschhauser, A., Lesur, V., & Grott, M. (2014). A spherical harmonic model of the lithospheric magnetic field of Mars. *Journal of Geophysical Research*, *119*, 1162–1188. https://doi.org/10.1002/2013JE004555

Němec, F., Morgan, D., Gurnett, D., Duru, F., & Truhlík, V. (2011). Dayside ionosphere of Mars: Empirical model based on data from the MARSIS instrument. *Journal of Geophysical Research*, *116*, E07003. https://doi.org/10.1029/2010JE003789

Nielsen, E., Zou, H., Gurnett, D. A., Kirchner, D. L., Morgan, D. D., Huff, R., … Picardi, G. (2007). Observations of vertical reflections from the topside Martian ionosphere. In C. T. Russell (Ed.), *The Mars plasma environment* (pp. 373–388). New York: Springer. https://doi.org/10.1007/978-0-387-70943-7_15

Nier, A., & McElroy, M. B. (1977). Composition and structure of Mars' upper atmosphere: Results from the neutral mass spectrometers on Viking 1 and 2. *Journal of Geophysical Research*, *82*(28), 4341–4349.

Oppenheim, M. (1997). Evidence and effects of a wave-driven nonlinear current in the equatorial electrojet. *Annales Geophysicae*, *15*, 899–907.

Pätzold, M., Tellmann, S., Häusler, B., Hinson, D., Schaa, R., & Tyler, G. (2005). A sporadic third layer in the ionosphere of Mars. *Science*, *310*(5749), 837–839.

Picardi, G., Biccari, D., Seu, R., Plaut, J., Johnson, W., Jordan, R., … Zampolini, E. (2004). *MARSIS: Mars advanced radar for subsurface and ionosphere sounding*.

Prakash, S., Subbaraya, B., & Gupta, S. (1972). Rocket measurements of ionization irregularities in the equatorial ionosphere at Thumba & identification of plasma instabilities. *Indian Journal of Radio & Space Physics*, *1*, 72.

Savich, N. A., & Samovol, V. A. (1976). The night time ionosphere of Mars from Mars 4 and Mars 5 dual-frequency radio occultation measurements. In M. J. Rycroft (Ed.), *Space research XVI* (pp. 1009–1011). Berlin, East Germany.

Schunk, R., & Nagy, A. (2009). *Ionospheres: Physics, plasma physics, and chemistry*. Cambridge, UK: Cambridge University Press.

Smith, L., & Klaus, D. (1978). Rocket observations of electron density irregularities in the equatorial E region. *Space Research XVIII*, *18*, 261–264.

Verigin, M., Gringauz, K., Shutte, N., Haider, S., Szego, K., Kiraly, P., … Gombosi, T. (1991). On the possible source of the ionization in the nighttime Martian ionosphere: 1. Phobos 2. HARP electron spectrometer measurements. *Journal of Geophysical Research*, *96*(A11), 19,307–19,313.

Withers, P., Mendillo, M., Rishbeth, H., Hinson, D. P., & Arkani-Hamed, J. (2005). Ionospheric characteristics above Martian crustal magnetic anomalies. *Geophysical Research Letters*, *32*, L16204. https://doi.org/10.1029/2005GL023483

Zhang, M., Luhmann, J., & Kliore, A. (1990). An observational study of the nightside ionospheres of Mars and Venus with radio occultation methods. *Journal of Geophysical Research*, *95*(A10), 17,095–17,102.